Organic Electronics 11 (2010) 925–932

Contents lists available at ScienceDirect

Organic Electronics

journal homepage: www.elsevier.com/locate/orgel

Optimization of poly(vinylidene fluoride-trifluoroethylene) films as non-volatile memory for flexible electronics

D. Mao [a], M.A. Quevedo-Lopez [a,*], H. Stiegler [a], B.E. Gnade [a], H.N. Alshareef [b]

[a] Department of Material Science and Engineering, The University of Texas at Dallas, Richardson, TX 75080, USA
[b] Department of Material Science and Engineering, King Abdullah University of Science and Technology, Jeddah, Saudi Arabia

ARTICLE INFO

Article history:
Received 26 December 2009
Received in revised form 14 February 2010
Accepted 17 February 2010
Available online 21 February 2010

Keywords:
Flexible electronics
Ferroelectric polymer
Non-volatile memory
P(VDF-TrFE)

ABSTRACT

The impact of thermal treatment and thickness on the polarization and leakage current of poly(vinylidene fluoride-trifluoroethylene) [P(VDF-TrFE)] copolymer thin film capacitors has been studied. The evolution of the film morphology, crystallinity and bonding orientation as a function of annealing temperature and thickness were characterized using multiple techniques. Electrical performance of the devices was correlated with the material properties. It was found that annealing at or slightly above the Curie temperature (T_c) is the optimal temperature for high polarization, smooth surface morphology and low leakage current. Higher annealing temperature (but below the melting temperature T_m) favors larger size β crystallites through molecular chain self-organization, resulting in increased film roughness, and the vertical polarization tends to saturate. Metal–Ferroelectric–Metal (MFM) capacitors consistently achieved P_s, P_r and V_c of 8.5 μC/cm^2, 7.4 μC/cm^2 and 10.2 V, respectively.

Published by Elsevier B.V.

1. Introduction

Electrically addressable non-volatile memory is a key component for integrated logic circuits for flexible electronics. Ferroelectric Random Access Memory (FRAM) based on ferroelectric polymers is a leading candidate because of the compatibility with low temperature (<150 °C) plastic substrates, low-operating voltage, long data retention time, and fast readout. Poly(vinylidene fluoride-trifluoroethylene) [P(VDF-TrFE)] copolymer is one of the most popular ferroelectric polymers for memory applications due to its excellent electrical switching behavior as well as chemical stability [1–3]. Poly(vinylidene fluoride-trifluoroethylene) based capacitors can also be integrated with flexible complementary metal oxide semiconductor devices [4].

The high polarization of the poly(vinylidene fluoride-trifluoroethylene) copolymer originates from the large difference in electronegativity between fluorine, carbon and hydrogen (Pauling's value for fluorine, carbon and hydrogen are 4.0, 2.5 and 2.1, respectively) [5]. Most of the electrons are attracted to the fluorine side of the chain and polarization is created [6,7]. Similar to poly(vinylidene fluoride) [PVDF], poly(vinylidene fluoride-trifluoroethylene) has four known phases; phase I (β), phase II (α), phase III (γ) and phase IV (δ) [8]. The β phase is the all-trans zig-zag planar configuration, which generates the largest polarization along the *b* axis (parallel to C, F dipole moment) [9]. The amount of each phase can be controlled through deposition method and thermal treatment history. Also, a proper concentration of TrFE in the copolymer helps to increase and stabilize the β phase [10].

Many studies have focused on the film morphology, phase transition, crystallinity, thickness, and thermal annealing [10–14]. A detailed correlation between the film properties and electrical performance vs. different annealing temperatures has not been reported. High leakage current has been a significant problem that limits this material as a viable option for flexible electronics [15]. We report the impact of annealing temperature and film thickness on poly(vinylidene fluoride-trifluoroethylene)

* Corresponding author. Tel.: +1 972 883 5714; fax: +1 972 883 5725.
E-mail address: mquevedo@utdallas.edu (M.A. Quevedo-Lopez).

1566-1199/$ - see front matter Published by Elsevier B.V.
doi:10.1016/j.orgel.2010.02.012

film characteristics, and correlate the material properties with MFM device performance. These results demonstrate that through careful film processing this material may be a promising solution for a non-volatile memory element for flexible electronics.

2. Experimental

Metal–Ferroelectric–Metal capacitors were fabricated as follows. P(VDF-TrFE) copolymer powder with 70/30 mol ratio (Hisense Electronics Co., China) was dissolved in 2-butanone without further purification as 3 and 4 wt.%, respectively. Chromium and gold (10/100 nm) were e-beam evaporated on a silicon substrate with a Si_3N_4 buffer layer as the bottom contact, and patterned using photolithography. Copolymer films (154 and 210 nm) were then spin-coated on the Cr/Au contact from the 3 and 4 wt.% solutions, followed by drying and annealing at 65 °C, 118 °C, 133 °C, 144 °C and 156 °C (T_m is approximately 148 °C) for 2 h in a vacuum oven (pressure was approxi-

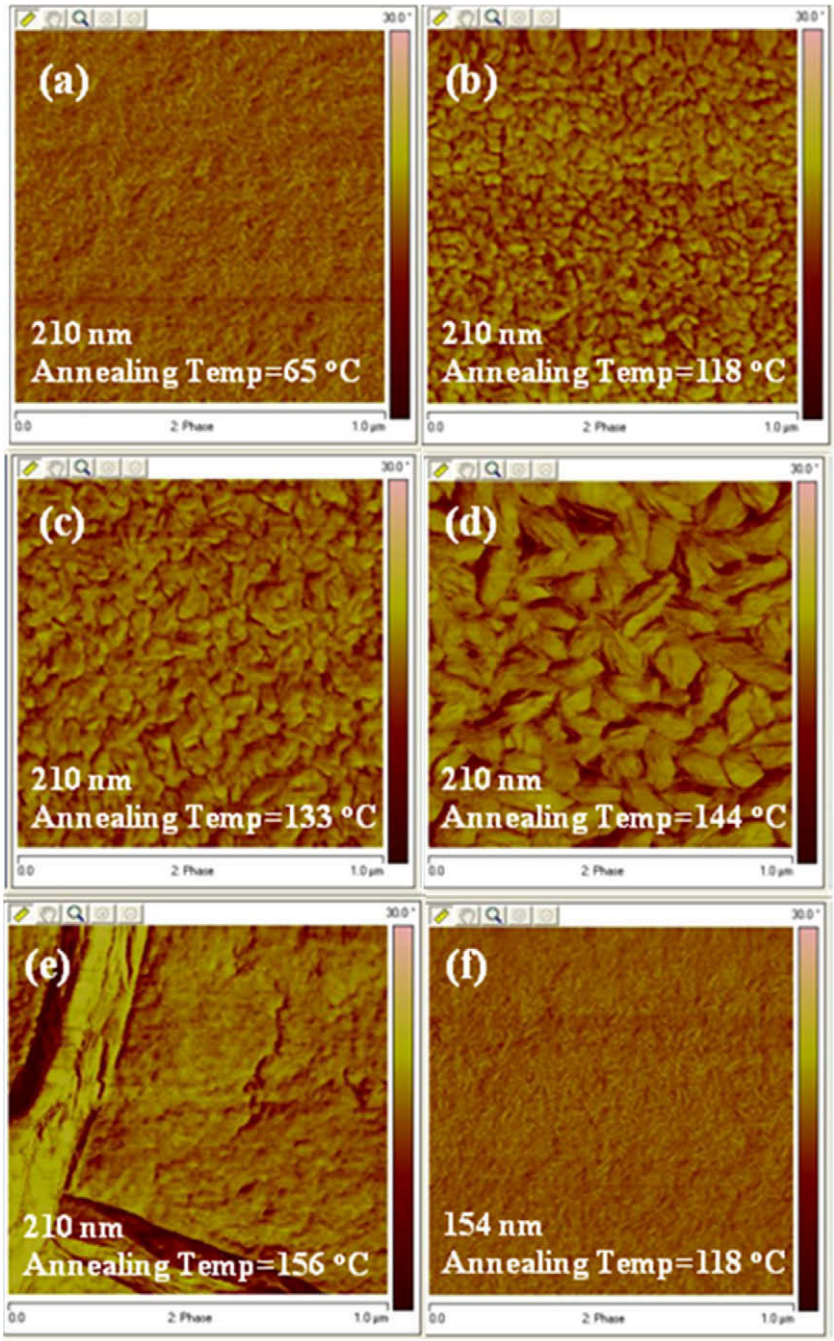

Fig. 1. (a)–(e) AFM phase images of 210 nm P(VDF-TrFE) films annealed from 65 °C to 156 °C and (f) shows 154 nm film annealed at 118 °C for comparison.

mately 20 Torr). All the samples were then left in the vacuum oven to slowly cool down to room temperature in order to maximize their grain size. Gold was thermally evaporated and photolithography patterned on the copolymer film as the top contact. The area of the MFM capacitors ranged from 0.0003 cm^2 to 0.0025 cm^2. The electrical performance was characterized using Capacitance–Voltage (HP4284, Agilent), Displacement Current–Voltage (Keithley 4200 semiconductor parameter analyzer), and Displacement Charge Density–Voltage (virtual ground circuit, RT66B, Radiant Technology). Film thicknesses were determined using a profilometer (Dektak), surface morphology was studied using Atomic Force Microscopy (AFM, DM09 Veeco), crystallinity was measured using thin film X-ray diffraction (XRD, Rigaku), and molecular bonding and orientation were characterized using Fourier-transform infrared reflection–absorption spectroscopy (FT-IR, Magna-IR 560, Nicolet). The ferroelectric β phase increases with annealing temperature. We demonstrate that high polarization and low leakage current can be achieved by annealing at, or slightly above T_c, whereas annealing at higher temperature, but below the melting temperature increases leakage current.

3. Results and discussions

To correlate the film's physical and chemical characteristics with device performance, P(VDF-TrFE) films were studied before top electrode deposition. We studied the microstructure, surface morphology, crystallinity and molecular phase configuration. Fig. 1a–e shows the AFM phase images (tapping mode) of 210 nm films annealed at temperatures ranging from 65 °C to 156 °C. Films annealed at 65 °C, below the Curie temperature (T_c = 118 °C), show a smooth surface with relatively small grain size (Fig. 1a). As the annealing temperature increases near, and above T_c (Fig. 1b and c), the polymer grain size increases, as expected. Films annealed at 144 °C (just below T_m = 148 °C) show the largest grain size (approximately 180 nm long) (Fig. 1d). Annealing at temperatures above T_m at 156 °C, results in films with a completely different morphology. This is due to film re-crystallization during cooling [11,16]. We also compare 154 nm (Fig. 1e) with 210 nm films (Fig. 1b) annealed using the same conditions. While the thinner films follow the same trend as thicker films (Fig. 2a), it can be seen that the thinner film shows smaller grains, even though the films are annealed using the same conditions and temperature. This indicates that P(VDF-TrFE) crystallization is a function of not only the annealing temperature, but also film thickness, and demonstrates that annealing has to be optimized for each film thickness. The evolution of film roughness as a function of annealing temperature and film thickness is shown in Fig. 2b. It is well known that P(VDF-TrFE) copolymer is a polycrystalline material, and that its ferroelectric response is attributed to the β phase (all-trans), which shows a rod-like shape with a relatively rough surface [15]. Fig. 2b shows a clear increase in the Root-Mean-Square (RMS) roughness as a function of annealing temperature, suggesting the presence of the β phase. Although higher annealing temperature favors

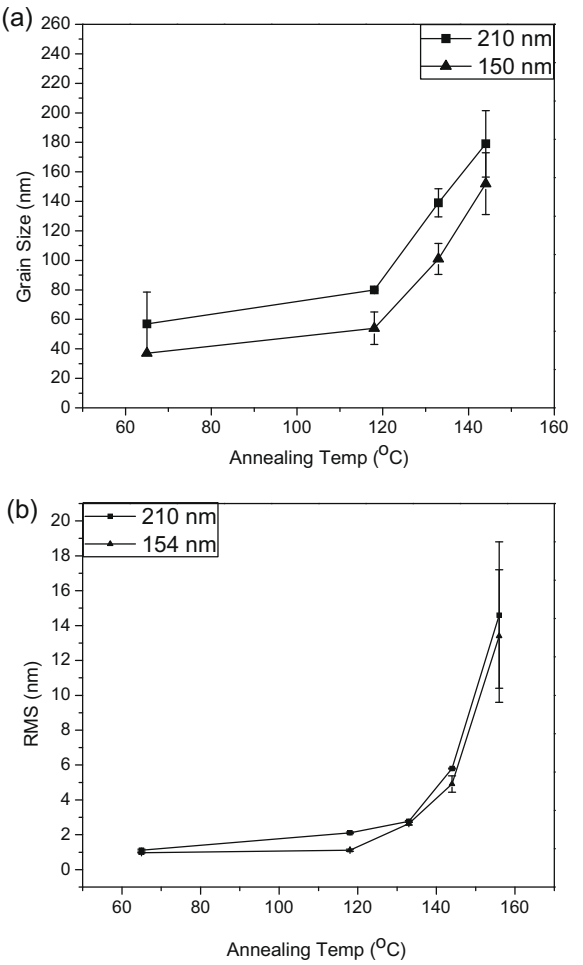

Fig. 2. (a) Average β phase crystallite grain size of 210 nm and 154 nm film at different annealing temperature treatment below T_m. (b) Surface roughness (RMS) of 210 nm and 154 nm films at different annealing temperatures.

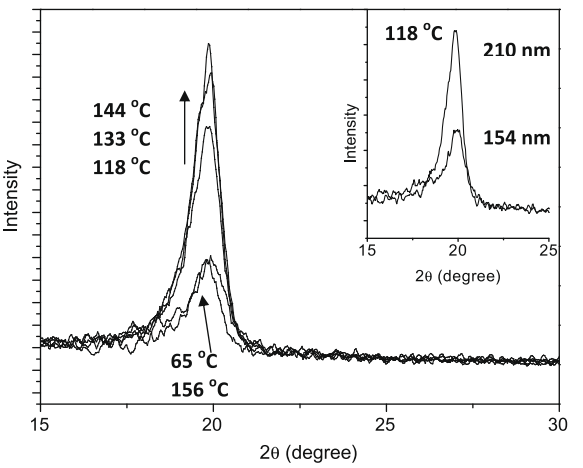

Fig. 3. XRD of 210 nm P(VDF-TrFE) films annealed at different temperatures. Inset shows both of the 210 nm and 154 nm films annealed at 118 °C.

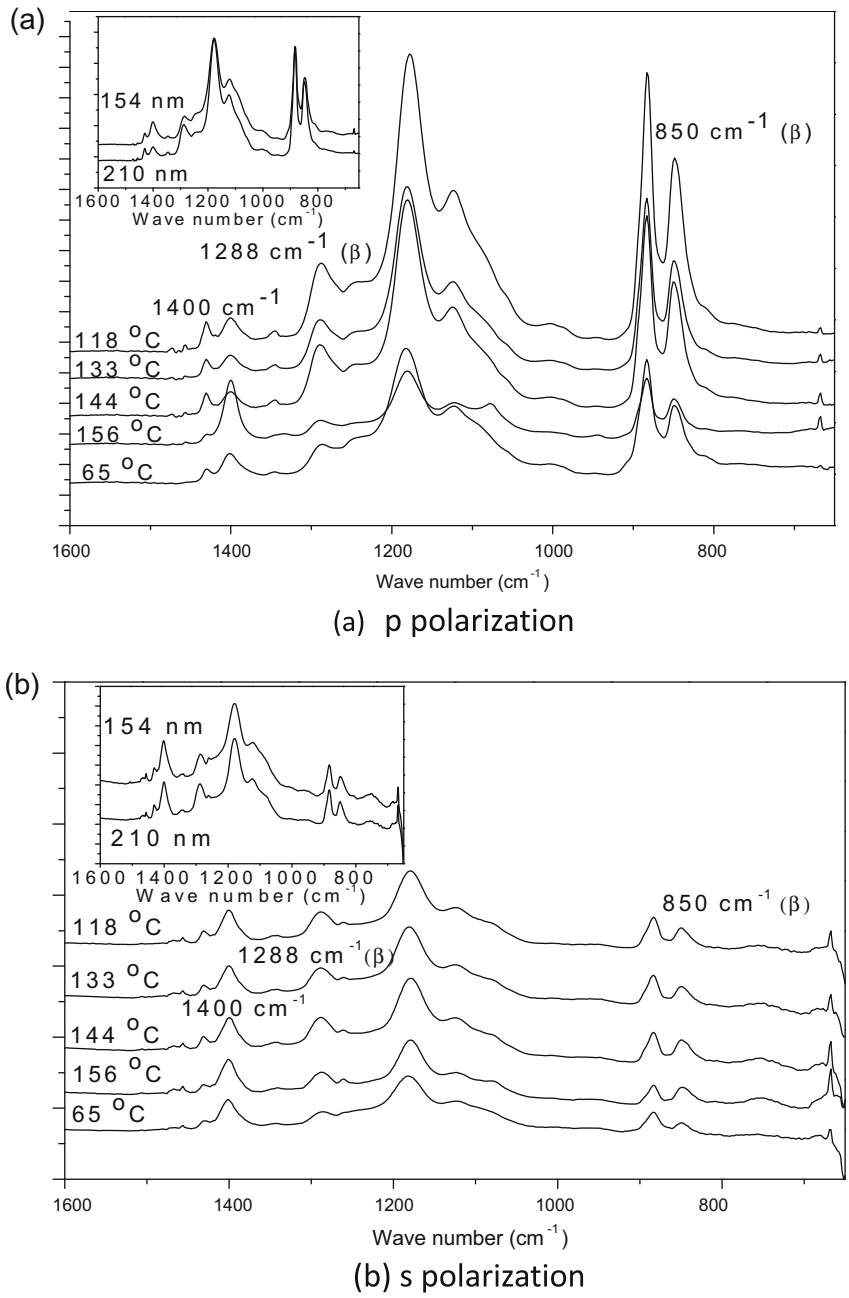

Fig. 4. (a) p Polarization (for molecular dipole interaction with direction perpendicular to substrate) and (b) s polarization (for molecular dipole interaction with direction parallel to substrate) of FT-IR of 210 nm P(VDF-TrFE) films annealed at different temperatures. Inset shows both of the 210 nm and 154 nm films annealed at 118 °C.

larger crystallites, it also increases surface roughness, which could result in increased leakage current. The RMS roughness increases from 1.1 nm to 14.6 nm for 210 nm films and from 1.0 nm to 13.4 nm for 154 nm films, as shown in Fig. 2.

Fig. 3 shows XRD results for the 210 nm films annealed at different temperatures. The sharp peak at $2\theta = 19.9°$ is assigned to the (1 1 0) and (2 0 0) orientations, and is attributed to the ferroelectric β phase. The diffraction angle of this peak does not change with the annealing conditions, indicating similar inter-chain spacing for all the annealing conditions [17]. The inter-planar distance was calculated to be approximately 4.5 Å, in agreement with an earlier report [10]. Higher annealing temperatures, but below T_m, produces more intense diffraction peaks, indicating a higher degree of crystallinity. Annealing above T_m causes a dramatic reduction in the peak intensity for the (1 1 0) and (2 0 0) peaks, which suggests a change in the crystalline

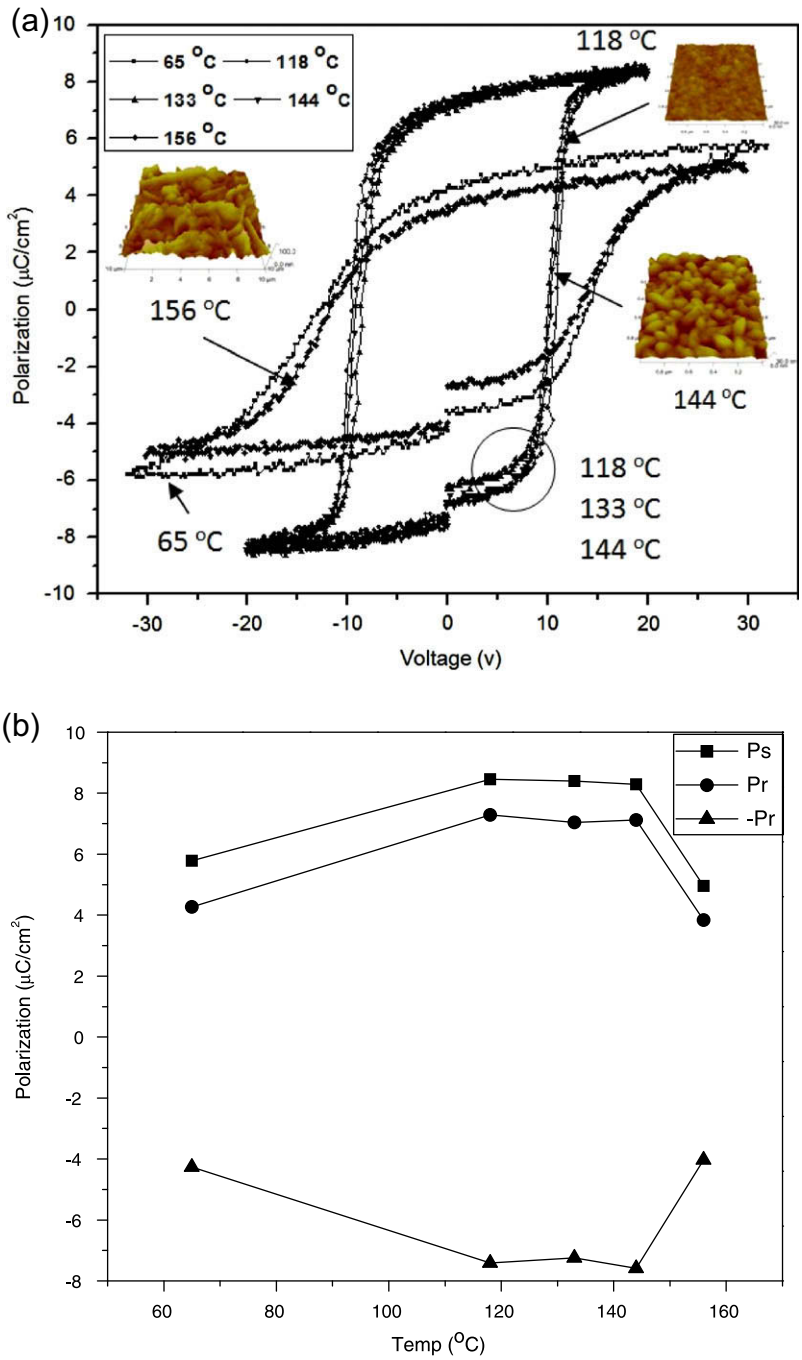

Fig. 5. (a) Hysteresis loops of 210 nm P(VDF-TrFE) copolymer films annealed at different temperatures. Inset AFM images show the morphologies of corresponding temperature annealed devices. (b) Saturation and remanent polarizations at different temperatures.

characteristics of the films, with a likely reduction in the ferroelectric β phase. The 154 nm films follow a similar trend. The 210 nm film shows a higher degree of crystallinity, as shown in the inset of Fig. 3.

Polarized FT-IR is used to characterize the localized chain orientation and configuration of the P(VDF-TrFE) films. We use the fact that the different P(VDF-TrFE) phases have different responses to the external electromagnetic field associated with FT-IR spectroscopy [18]. The large dipoles in P(VDF-TrFE) strongly interact with the applied IR electric field when the field is perpendicular to the dipole direction. Fig. 4a shows the FT-IR results (from 1600 cm^{-1} to 650 cm^{-1}) for 210 nm thick films annealed at different temperatures. IR with the electric field component parallel to the plane of the substrate (p polarization) is used for this measurement. The 1288 cm^{-1} and

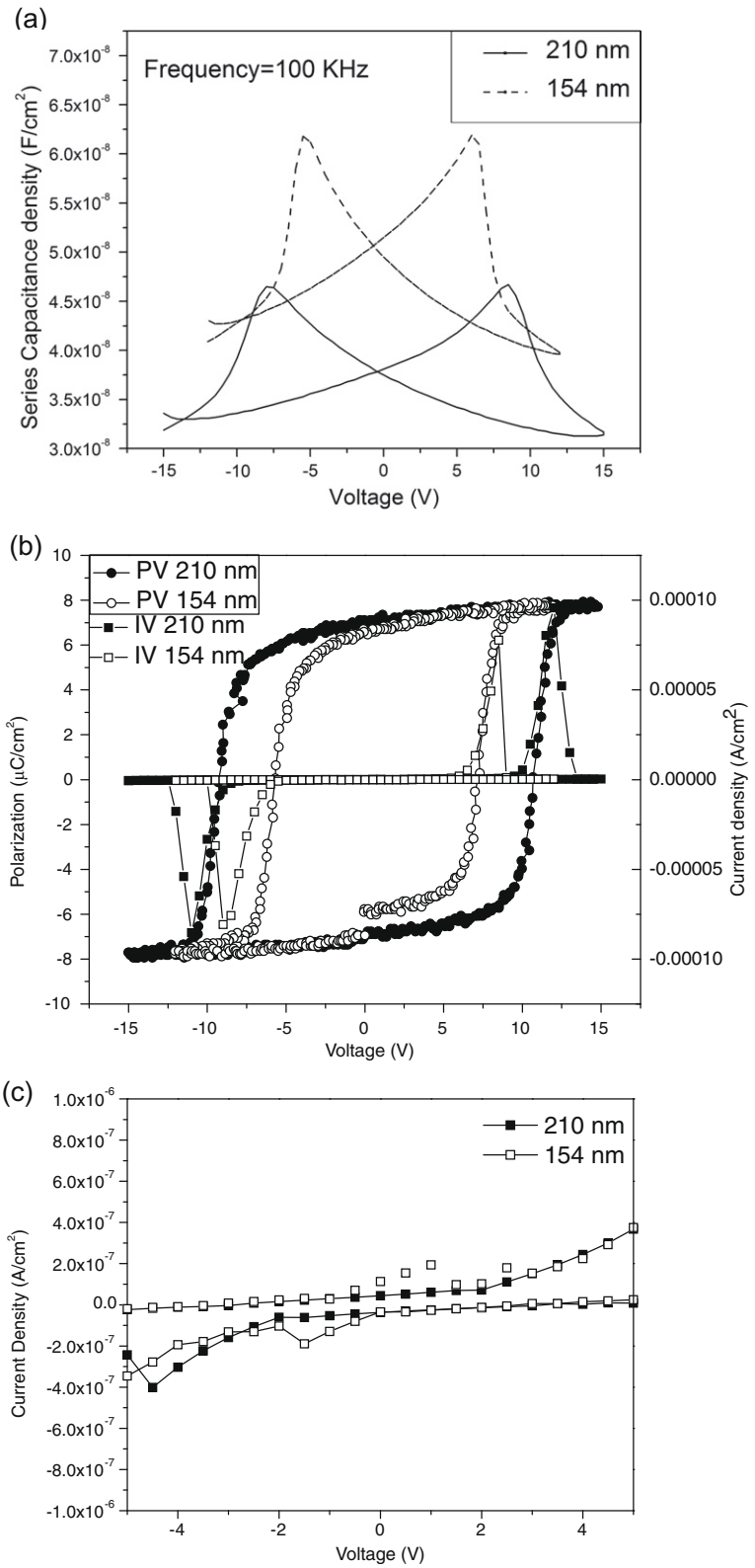

Fig. 6. (a) *C–V* measured at 100 kHz, (b) *P–V* and *I–V* data and (c) Leakage current for low voltage sweep for 210 nm and 154 nm P(VDF-TrFE) MFM devices annealed at 118 °C.

850 cm^{-1} bands are assigned to CF_2 symmetric stretching characteristics of the β phase, with three or more trans sequence of isomers [19]. These IR absorption bands indicate transition dipole moments μ parallel to the polar *b* axis [9]. For samples annealed at 118 °C, 133 °C and 144 °C, these two absorption bands can be clearly seen, indicating that the *b* axis of the copolymer film is perpendicular to the substrate. For the samples annealed at 65 °C and 156 °C, these two bands are relatively weak, indicating that the *b* axis is tilted away from the direction normal to the surface. Moreover, the 1400 cm^{-1} band (the wagging vibration of CH_2), which has μ parallel to the polymer chain *c* axis, increases for the film annealed above T_m, indicating that a significant portion of the copolymer chain tilts vertically, which is undesirable for vertical polarization [20]. In contrast, s polarized (the electric field component is perpendicular to the substrate) IR spectra of samples annealed at low temperature (Fig. 4b) show a large absorption ratio between 1400 cm^{-1} and 1288 cm^{-1} bands, indicating the strong wagging vibration of CH_2 along the *c* axis, and confirming that most of the copolymer chains are oriented parallel to the substrate when the films are annealed below T_m.

The electrical performance of the devices with area of 0.0005 cm^2 was evaluated after fabrication as a function of annealing conditions and film thickness. The Polarization–Voltage (*P*–*V*) hysteresis loops (1 Hz) for 210 nm MFM devices with different annealing temperatures measured at room temperature are shown in Fig. 5a. For devices annealed at 65 °C, PV shows a saturation polarization (P_s) of 5.8 μC/cm^2 and a remanent polarization (P_r) of 4.3 μC/cm^2 with a coercive voltage (V_c) of approximately 13.3 V (corresponding to a coercive field E_c = 0.63 MV/cm). These data are for a voltage sweep from −32 V to 32 V (*E* field of −1.52 MV/cm to 1.52 MV/cm). The low polarization and high V_c are consistent with a low concentration of the ferroelectric β phase, as confirmed by the AFM, FT-IR and XRD results. When the annealing temperature is increased to 118 °C, the polarization increases sharply, with a concurrent decrease of V_c. The *P*–*V* loops show a typical square shape with P_s, P_r and V_c of 8.5 μC/cm^2, 7.4 μC/cm^2 and 10.2 V, respectively. This corresponds to an E_c of approximately 0.5 MV/cm (measured at ±20 V for a field of ±0.95 MV/cm). These results are in agreement with previous reports [21]. The polarization saturates and the hysteresis loops remain almost constant as the annealing temperature increases to 133 °C and 144 °C. This saturation demonstrates that, although the grain size is different for each of these temperatures, annealing these films at 118 °C is enough to achieve acceptable ferroelectric performance. As the annealing temperature increases above T_m to 156 °C, P_s and P_r decrease, while V_c increases. This indicates the tilted chain orientation and a reduction of the ferroelectric β phase. This is also in agreement with changes in morphology seen with AFM, XRD and FT-IR. The discontinuities at the origin of the hysteresis loops are due to non-switchable polarization, as reported in Ref. [22].

P_s, P_r and $-P_r$ for the different annealing temperatures are plotted in Fig. 5b. While most of the polarization of P(VDF-TrFE) originates from the β phase, the β phase crystal orientation also impacts polarization [20]. The data suggest that annealing at temperatures equal to or slightly above T_c is sufficient to align the β phase dipole moment (μ) perpendicular to the substrate, which is the requirement for high P_s and P_r and low V_c. Although annealing at temperatures higher than T_c, but below T_m favors a higher degree of crystallinity with larger grains, the increased film roughness (Fig. 2) might be an issue for leakage current. The high surface roughness will cause a non-uniform electric field, with the concomitant increase in leakage current in the film. This will result in devices with lower electrical stability. Therefore, the best annealing temperature is at, or just above T_c.

Fig. 6 shows the *C*–*V*, *P*–*V* and *I*–*V* plots for 210 nm and 154 nm films annealed at 118 °C. Hysteresis was measured at ±15 V and ±12 V, respectively. Fig. 6a shows peak capacitance densities of 47 nF/cm^2 (210 nm) and 62 nF/cm^2 (154 nm), measured at 100 kHz. The dielectric constants of the films with the two thicknesses show similar values, between 7.8 and 11 depending on the measurement voltage, slightly higher than the value reported in the literature [21], probably due to the improved annealing treatment. The polarizations were measured to be 7.7 μC/cm^2 and 7.0 μC/cm^2 for P_s and P_r with a peak switching current of approximately 85 μA/cm^2 (Fig. 6b). The leakage current is lower than 5×10^{-7} A/cm^2 before the electric field reaches E_c (Fig. 6c). The maximum polling slope (d*P*/d*V*) of the two thicknesses of the devices shows similar values and the coercive field is consistent, indicating similar switching behavior. This indicates that film orientation might be more important that grain size. For the same annealing conditions, thicker films show larger grains, but the electrical performance of the films is similar for different thicknesses.

4. Conclusion

The transition of the β phase crystallite and the rearrangement of the molecular chain orientation to favor vertical ferroelectric polarization can be achieved with thermal annealing at or just above T_c. The polarization of the MFM devices after bias tends to saturate as annealing temperature increases. Higher annealing temperature (but below T_m) results in films with larger grains, higher degree of crystallinity and increased roughness, but less effect on molecular chain orientation. Annealing above the T_m, results in a shift of molecular chain orientation, degraded β phase crystallization and decreased polarization. Thicker films produce larger grains and a higher degree of crystallinity, however, the polarization does not increase because it is more related to molecular orientation. When reducing the thickness of the film, the annealing process needs to be optimized to reach high polarization as well as smooth surface morphology. We conclude that annealing at or slightly above T_c for the P(VDF-TrFE) copolymer is optimal to achieve maximum polarization and low leakage, and is compatible with low temperature substrates for flexible electronics applications.

Acknowledgements

The authors thank the Army Research Laboratory (ARL) for partial financial support of this project. We would also

like to thank Dr. Eric Forsythe of ARL for very helpful discussions regarding non-volatile memory integration.

References

[1] R.C.G. Naber, C. Tanase, P.W.M. Blom, G.H. Gelinck, A.W. Marsman, F.J. Touwslager, S. Setayesh, D.M. de leeuw, Nat. Mater. 4 (2005) 243.
[2] R.C.G. Naber, P.W.M. Blom, A.W. Marsman, D.M. de Leeuw, Appl. Phys. Lett. 85 (2004) 2032.
[3] G.H. Gelinck, A.W. Marsman, F.J. Touwslager, S. Setayesh, D.M. de Leeuw, R.C.G. Naber, P.W.M. Blom, Appl. Phys. Lett. 87 (2005) 092903.
[4] S. Gowrisanker, M.A. Quevedo-Lopez, H.N. Alshareef, B.E. Gnade, S. Venugopal, R. Krishna, K. Kaftanoglu, D.R. Allee, Org. Electron. 10 (2009) 1217.
[5] L. Pauling, The Nature of the Chemical Bonding, third ed., Cornell University Press, Ithaca, NY, 1960, p. 644.
[6] S. Fujisaki, H. Ishiwara, Y. Fujisaki, Appl. Phys. Lett. 90 (2007) 162902.
[7] A. Salimi, A.A. Yousefi, J. Polym. Sci.: Part B: Polym. Phys. 42 (2004) 3487.
[8] H.S. Xu, G. Shanthi, V. Bharti, Q.M. Zhang, Macromolecules 33 (2000) 4125.
[9] Z.J. Hu, M.W. Tian, B. Nysten, A. Jonas, Nat. Mater. 8 (2009) 62.
[10] T. Yamada, T. Kitayama, J. Appl. Phys. 52 (1981) 6859.
[11] W.P. Li, Y.J. Zhu, D.Y. Hua, P.Q. Wang, X.R. Chen, J. Shen, Appl. Surf. Sci. 254 (2008) 7321.
[12] T. Yamada, T. Ueda, T. Kitayama, J. Appl. Phys. 52 (1981) 948.
[13] K. Urayama, M. Tsuji, D. Neher, Macromolecules 33 (2000) 8269.
[14] I. Lazareva, Y. Koval, P. Müller, K. Müller, K. Henkel, D. Schmeisser, J. Appl. Phys. 105 (2009) 054110.
[15] R.C.G. Naber, B. de Boer, P.W.M. Blom, D.M. de Leeuw, Appl. Phys. Lett. 87 (2005) 203509.
[16] F.J. Baltá Calleja, A. González Arche, T.A. Ezquerra, C. Santa Cruz, F. Batallán, B. Frick, E. López Cabarcos, Adv. Polym. Sci. 108 (1993) 1.
[17] H.S. Xu, X.B. Liu, X.R. Fang, H.F. Xie, G.B. Li, X.J. Meng, J.L. Sun, J.H. Chu, J. Appl. Phys. 105 (2009) 034107.
[18] K.J. Kim, N.M. Reynolds, S.L. Hsu, Macromolecules 22 (1989) 4395.
[19] N.M. Reynolds, K.J. Kim, C. Chang, S.L. Hsu, Macromolecules 22 (1989) 1092.
[20] Y.J. Park, S.J. Kang, C. Park, K.J. Kim, H.S. Lee, M.S. Lee, U.I. Chung, I.J. Park, Appl. Phys. Lett. 88 (2006) 242908.
[21] K.H. Lee, G. Lee, K. Lee, M.S. Oh, S. Im, Appl. Phys. Lett. 94 (2009) 093304.
[22] A.K. Tagantsev, I. Stolichnov, E.L. Colla, N. Setter, J. Appl. Phys. 90 (2001) 1387.